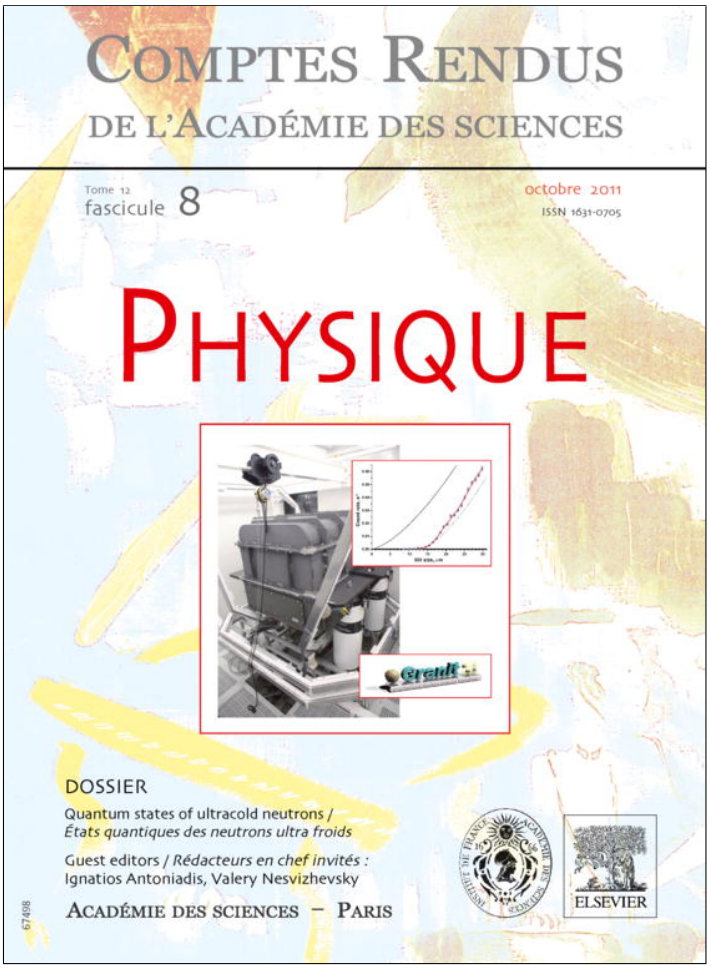

C. R. Physique 12 (2011) 779–790

Contents lists available at SciVerse ScienceDirect

Comptes Rendus Physique

www.sciencedirect.com

Ultra cold neutron quantum states / États quantiques des neutrons ultra froids

# Quantum phenomena in gravitational field

## *Phénomènes quantiques dans le champ gravitationnel*

Th. Bourdel [a], M. Doser [b], A.D. Ernest [c], A.Yu. Voronin [d,*], V.V. Voronin [e]

[a] *Laboratoire Charles-Fabry de l'Institut d'Optique, CNRS, Univ. Paris-Sud, Campus Polytechnique RD128, 91127 Palaiseau, France*
[b] *CERN, Geneva 23, CH-1211, Switzerland*
[c] *Faculty of Science, Charles Sturt University, Wagga Wagga, Australia*
[d] *Lebedev Institute, 53 Leninskii pr., Moscow, RU-119991, Russia*
[e] *PNPI, Orlova Roscha, Gatchina, RU-188300, Russia*

ARTICLE INFO

*Article history:*
Available online 9 September 2011

*Keywords:*
Quantum phenomena
Gravitational field
Experimental methods

*Mots-clés :*
Phénomènes quantiques
Champ gravitationnel
Méthodes expérimentales

ABSTRACT

The subjects presented here are very different. Their common feature is that they all involve quantum phenomena in a gravitational field: gravitational quantum states of ultracold antihydrogen above a material surface and measuring a gravitational interaction of antihydrogen in AEGIS, a quantum trampoline for ultracold atoms, and a hypothesis on naturally occurring gravitational quantum states, an Eötvös-type experiment with cold neutrons and others. Considering them together, however, we could learn that they have many common points both in physics and in methodology.



RÉSUMÉ

Les sujets présentés ici sont très variés. Comme point commun, ils traitent tous de phénomènes quantiques dans un champ de gravitation : états quantiques gravitationnels de l'anti hydrogène ultra froid au-dessus d'une surface matérielle et mesure de l'interaction gravitationnelle de l'anti hydrogène avec AEGIS, trampoline quantique pour atomes ultra froids, hypothèse sur des états quantiques présents naturellement dans un champ de gravitation, expérience de type Eötvös avec des neutrons froids, et d'autres. En les considérant ensemble, on peut constater que ces divers sujets ont de nombreux points communs, tant au niveau de la physique en jeu que de la méthodologie.



## 1. Introduction

In contrast to other thematic days of the GRANIT-2010 workshop, the phenomena presented in this "Day-4" article are very diverse; also they were studied by different research groups.

Section 2 describes gravitational quantum states of ultracold antihydrogen atoms above a material surface, and Section 3 deals with measuring a gravitational interaction of antihydrogen atoms in AEGIS. Section 4 discusses a hypothesis on naturally occurring gravitational quantum states. A quantum trampoline for ultracold atoms is presented in Section 5. An Eötvös-type experiment with cold neutrons is analyzed in Section 6. Confinement-induced neutron phases are discussed in

* Corresponding author.
*E-mail address:* dr.a.voronin@gmail.com (A.Yu. Voronin).

1631-0705/$ – see front matter 
doi:10.1016/j.crhy.2011.08.001

Section 7. Other subjects discussed during GRANIT-2010 workshop but not included in this short overview include: test of the equivalence principle with ultracold neutrons, storage of ultracold neutrons in gravito-magnetic trap, and problems to measure confinement-induced neutron phases.

## 2. Quantum states of ultracold antihydrogen above material surface (Alexei Voronin)

In the context of the general relativity theory, universality of a free fall is often referred to as the Weak Equivalence Principle (WEP). WEP is being tested with increasing sensitivity for macroscopic bodies. The best test so far confirms WEP to the accuracy of $2\times10^{-13}$ (using a rotating torsion balance [1]). Ongoing projects aim at the accuracy of 1 part in $10^{18}$ (in an Earth orbiting satellite [2]). However, in view of difficulties in unifying quantum mechanics with the theory of gravity, it is of great interest to investigate the gravitational properties of quantum mechanical objects, such as elementary particles or atoms. Such experiments have already been performed, e.g. using interferometric methods to measure the gravitational acceleration of neutrons [3,4] and atoms [5–7]. The experiments with antiatoms (see [8,9] and references therein) are even more interesting in view of testing WEP, because the theories striving to unify gravity and quantum mechanics (such as super-symmetric string theories) tend to suggest violation of the gravitational equivalence of particles and antiparticles [10]. Experiments testing gravitational properties of antiatoms are on the agenda of all experimental groups working with antihydrogen (see e.g. ATHENA-ALPHA [11], ATRAP [12], and AEGIS [13]).

Here we investigate a possibility to explore gravitational properties of antiatoms in the ultimate quantum limit. We study antihydrogen atoms levitating in the lowest gravitational states above a material surface. The existence of such gravitational states for neutrons was proven experimentally [14–16]. The existence of analogous states for antiatoms is possible due to the effect of quantum reflection [17] of ultracold atoms from the Casimir–Polder atom–surface interaction potential [18,19]. We have shown that antihydrogen atoms, confined by the quantum reflection via Casimir forces from below, and by the gravitational force from above, would form meta-stable gravitational quantum states. They would bounce on a surface for a finite life-time of the order of 0.1 s [20–22].

The Schrödinger equation which governs antihydrogen dynamics in superposition of Casimir–Polder potential $V(z)$ (which has an asymptotic behavior $-\frac{C_4}{z^4}$ for large atom–surface separation $z$) and the gravitational potential $Mgz$ reads:

$$\left[-\frac{\hbar^2\partial^2}{2m\partial z^2}+V(z)+Mgz-E\right]\Psi(z)=0 \tag{1}$$

Here $m$ is the inertial mass, $M$ is the gravitational mass of $\bar{H}$, $g$ is the Earth's gravitational field strength near the surface. The above equation meets a boundary condition of full absorption of antiatoms in the bulk of material surface ($z=0$) [20]. The above equation establishes the following length and energy scales:

$$l_0=\sqrt[3]{\frac{\hbar^2}{2mMg}},\qquad l_{CP}=\frac{\sqrt{2mC_4}}{\hbar},\qquad \varepsilon_0=\sqrt[3]{\frac{\hbar^2M^2g^2}{2m}},\qquad \varepsilon_{CP}=\frac{\hbar^4}{4m^2C_4} \tag{2}$$

Here $l_0=5.871$ μm is the characteristic gravitational length scale, $l_{CP}=0.027$ μm is the characteristic Casimir–Polder interaction length scale, $\varepsilon_0=6.011\times10^{-13}$ eV is the characteristic gravitational energy scale, and $\varepsilon_{CP}=2.739\times10^{-8}$ eV is the Casimir–Polder energy scale. As one can see, the gravitational length scale is much larger than the Casimir–Polder length scale $l_0\gg l_{CP}$, while the gravitational energy scale is much smaller than the Casimir–Polder energy scale $\varepsilon_0\ll\varepsilon_{CP}$. It is essential that for the characteristic energies of interest ($E\sim\varepsilon_0$) the effect of Casimir–Polder potential and the antiatoms annihilation in the material wall can be described by only one complex parameter, namely the complex scattering length, calculated in [20]:

$$a_{CP}=-(0.10+i1.05)l_{CP}=-0.0027-i0.0287\ \mu\text{m} \tag{3}$$

Indeed, in such a case the condition of scattering length approximation validity $|\sqrt{2mE}a_{CP}|\ll1$ is met. The effect of quantum reflection consists in over-barrier reflection of atoms from the rapidly changing (asymptotic) tail of Casimir–Polder potential, the reflection probability $|S|^2$ in our low energy case is given by:

$$|S|^2\approx1-4\sqrt{2mE}|Ima_{CP}|/\hbar \tag{4}$$

As one can see, the reflection probability tends to unity in zero energy limit. It reaches 95% for antihydrogen energy $E=10^{-12}$ eV, 70% for $E=10^{-10}$ eV, 30% for $E=10^{-9}$ eV. The hierarchy of the Casimir–Polder and gravitational scales $l_{CP}\ll l_0$ suggests that the energy levels of antihydrogen in the gravitational field in presence of the Casimir–Polder potential can be obtained by the following simple modification of the quantum bouncer (i.e. a particle bouncing in the gravitational field above a reflecting mirror [23]) energy levels:

$$E_n=E_n^0+Mga_{CP},\quad E_n^0=Mgl_0\lambda_n^0 \tag{5}$$

Here $\lambda_n^0$ is the quantum bouncer eigenvalue, which satisfies the equation

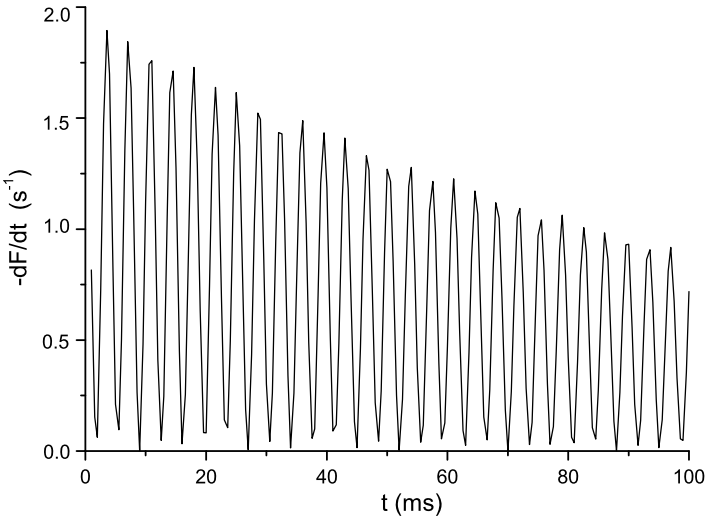


**Fig. 1.** Evolution of the annihilation rate of $\overline{H}$ atom in a superposition of first and second gravitational states.

**Fig. 1.** Evolution du taux d'annihilation d'atomes $\overline{H}$ dans une superposition du premier et du deuxième état quantique dans le potentiel de gravitation.

$$Ai\left(-\lambda_n^0\right) = 0 \tag{6}$$

Here $Ai(z)$ is the Airy function [24]. The negative imaginary part of the scattering length gives the width of the gravitational states:

$$\frac{\Gamma}{2} = Mg|Ima_{CP}| \tag{7}$$

An important message from Eq. (5) is that the complex shift $Mga_{CP}$ (due to the account of quantum reflection on the Casimir–Polder potential) is the same for all low-lying quasi-stationary gravitational levels. It means that all states have the same width and the transition frequencies between the gravitational states are not affected by the Casimir–Polder interaction. In particular, the transition frequency between 2 lowest gravitational states is $\omega_{12} = 254.54$ Hz.

The decaying character of gravitational states gives rise to non-zero probability current through the surface $z = 0$, which determines the annihilation rate of bouncing antihydrogen. In case there is a superposition of a few gravitational states such current exerts beatings, corresponding to the gravitational energy level difference. In particular, for two lowest states superposition (see Fig. 1), the annihilation rate $\frac{\mathrm{d}F_{12}}{\mathrm{d}t}$ is:

$$\frac{\mathrm{d}F_{12}(t)}{\mathrm{d}t} = -\frac{\Gamma}{\hbar}\exp\left(-\frac{\Gamma}{\hbar}t\right)\left(1+\cos(\omega_{12}t)\right) \tag{8}$$

A measurement of the oscillation frequency $\omega_{12}$ would allow us to extract the following combination of the gravitational and inertial masses:

$$\frac{M^2}{m} = \frac{2\hbar\omega_{12}^3}{g^2(\lambda_2^0-\lambda_1^0)^3} \tag{9}$$

Under additional assumption of equality of known the inertial mass of hydrogen atom $m_H$ and that of antihydrogen, imposed by CPT, we get:

$$M = \sqrt{\frac{2m_H\hbar\omega_{12}^3}{g^2(\lambda_2^0-\lambda_1^0)^3}} \tag{10}$$

Full information could be obtained from additional measurements of the spatial density distribution of $\overline{H}$ in a superposition of gravitational states, for instance, in the flow-through experiments (a kind of a beam scattering experiment), in which $\overline{H}$ atoms with a broad horizontal velocity distribution move along the mirror surface. The time of flight along the mirror should be measured simultaneously with the spatial density distribution in a position-sensitive detector, placed at the mirror exit. Such a detector would be able to measure the density distribution along the vertical axis at a given time instant. The horizontal component of $\overline{H}$ motion could be treated classically. Due to a broad distribution of horizontal velocities in the beam, atoms would be detected within a wide range of time intervals between their entrance to the mirror and their detection at the exit. In such an approach, we could study the time evolution of $\overline{H}$ probability density at a given position $z$:

$$\left|\Phi_{(12)}(z,t)\right|^2 = \exp\left(-\frac{\Gamma}{\hbar}t\right)\left(\left|\Phi_{(12)}^{av}(z)\right|^2 + 2\mathrm{Re}\frac{Ai(z/l_0-\lambda_1)Ai(z/l_0-\lambda_2)}{Ai'(-\lambda_1)Ai'(-\lambda_2)}\exp(-i\omega_{12}t)\right)$$

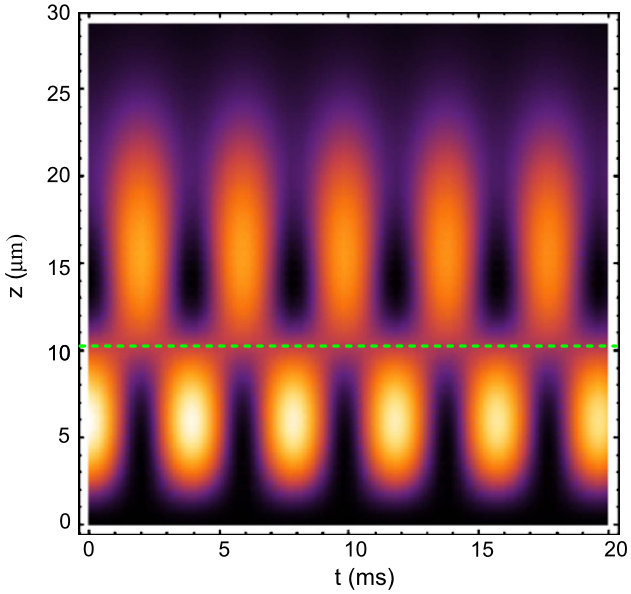


**Fig. 2.** The probability density of $\overline{H}$ in a superposition of the first and second gravitational states, as a function of the height $z$ above a mirror (vertical axis) and the time $t$ (horizontal axis). Dark shade: low probability density. Light shade: high probability density. The dashed line indicates the position of the node in the wave function of the second state.

**Fig. 2.** La densité de probabilité de $\overline{H}$ dans une superposition du premier et du deuxième état quantique dans le potentiel de gravitation, en fonction de la hauteur $z$ au dessus du miroir (axe vertical) et du temps $t$ (axe horizontal). Les zones sombres représentent une densité de probabilité faible et les zones claires une densité de probabilité elevée. La ligne discontinue indique la position du nœud de la fonction d'onde du deuxième état.

$$\left|\Phi^{av}_{(12)}(z)\right|^2 = \left|\frac{Ai(z/l_0-\lambda_1)}{Ai'(-\lambda_1)}\right|^2 + \left|\frac{Ai(z/l_0-\lambda_2)}{Ai'(-\lambda_2)}\right|^2 \tag{11}$$

The transition $\omega_{12} = 254.54$ Hz could be extracted from the probability density time evolution at a given $z$. The length scale $l_0$ could be extracted from the position of the zero $z_0$ of the second state wave function. Such a zero position is given by equation:

$$Ai(z_0/l_0-\lambda_2) = 0 \quad \Rightarrow \quad z_0 = l_0(\lambda_2-\lambda_1) \tag{12}$$

The probability density in Eq. (11) of two-states superposition at the height $z = z_0$ behaves like the probability density of the ground state alone (see Fig. 2):

$$\left|\Phi_{(12)}(z_0,t)\right|^2 = \exp\left(-\frac{\Gamma}{\hbar}t\right)\left|\frac{Ai(\lambda_2-\lambda_1)}{Ai'(-\lambda_1)}\right|^2 \tag{13}$$

From knowing the length $l_0$ and the energy $\varepsilon_0$ scales, one could get the following expressions for the inertial $m$ and gravitational $M$ masses of $\overline{H}$:

$$m = \frac{\hbar^2}{2\varepsilon_0 l_0^2}, \qquad M = \frac{\varepsilon_0}{g l_0} \tag{14}$$

The equality $m = M$ postulated by WEP relates $\varepsilon_0$ and $l_0$ as follows:

$$\varepsilon_0 = \hbar\sqrt{\frac{g}{2l_0}} \tag{15}$$

or, using the gravitational time scale $\tau_0 = \frac{\hbar}{\varepsilon_0}$:

$$\tau_0 = \sqrt{\frac{2l_0}{g}} \tag{16}$$

One can easily recognize in the above expression a classical time of fall from the height $l_0$ in the Earth's gravitational field.

## 3. Measuring the gravitational interaction of antihydrogen with AEGIS (Michael Doser)

Modern theories of gravity that attempt to unify gravity with the other forces of nature allow that, at least in principle, antimatter may fall differently from normal matter in the Earth's gravitational field, which would constitute a violation of

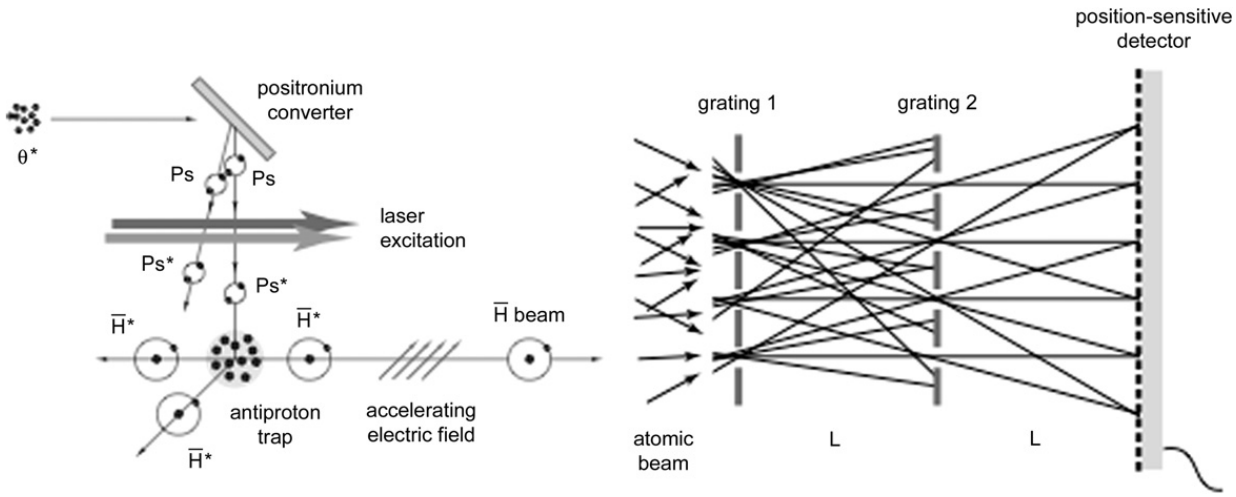


**Fig. 3.** Left: Proposed method for the production of a pulsed beam of cold $\overline{H}$ atoms; right: schematic of the Moiré deflectometer.

**Fig. 3.** A gauche : méthode proposée pour produire un faisceau pulsé d'atomes $\overline{H}$ froids ; à droite : schéma du déflectomètre de Moiré.

the weak equivalence principle. Specifically, as pointed out by Sherk [10] $N = 2, \ldots, 8$ theories of super-gravity (where $N$ is the number of super-symmetries) lead to the possibility of (massive, and thus finite range) Kaluza–Klein graviscalar and gravivector components to the gravitational interaction which may lead to different couplings for matter and antimatter. While it is possible to constrain deviations from standard gravity through e.g. effects of virtual antiparticles in ordinary matter [25–27] the behavior of antimatter particles in a gravitational field has never been tested experimentally. The recent production of large amounts of cold antihydrogen ($\overline{H}$) at CERN's Antiproton Decelerator (AD) [28,29] has paved the way for precision gravity experiments with neutral antimatter. The primary scientific goal of a consequently proposed AEGIS [30] experiment (Antimatter Experiment: Gravity, Interferometry, Spectroscopy) is the first direct measurement of the Earth's local gravitational acceleration $g$ on antihydrogen to 1%.

The essential steps leading to the production of a pulsed cold beam of antihydrogen and the measurement of $g$ with AEGIS are the following (Fig. 3):

- Production of positrons ($e^+$) from a Surko-type source and accumulator;
- Capture and accumulation of antiprotons ($\bar{p}$) from the AD in a cylindrical Penning trap;
- Cooling of the $\bar{p}$ to sub-K temperatures;
- Production of positronium ($Ps$) by bombardment of a cryogenic nanoporous material with an intense $e^+$ pulse;
- Excitation of the $Ps$ to a Rydberg state with principal quantum number $n = 30$–$40$;
- Pulsed formation of $\overline{H}$ by resonant charge exchange between Rydberg $Ps$ and cold $\bar{p}$;
- Pulsed formation of a horizontal $\overline{H}$ beam by Stark acceleration with inhomogeneous electric fields;
- Determination of $g$ by observing the vertical displacement (using a high-resolution position-sensitive detector) of the periodic shadow image produced by the passage of the $\overline{H}$ beam though a two-grating Moiré deflectometer.

The feasibility of the first two points has been conclusively demonstrated by the ATRAP and ATHENA Collaborations [31,32]. Cooling antiprotons to $K$ temperatures has been demonstrated recently [33], while reaching lower temperatures will likely require further techniques, such as resistive cooling, or sympathetic cooling [34].

In recent years, nanoporous insulator materials have been studied as highly efficient $Ps$ converters [35]. A sizable fraction of the $Ps$ formed by implanting $e^+$ in such a material at ∼keV energies diffuses out of the film after collision-induced thermalization. The overall ortho-$Ps$ yield (as well as the final velocity distribution) depends upon the characteristics of the target material (in particular, its pore structure), the implantation depth, and the target temperature. For the AEGIS experiment, the precise degree of thermalization is critical, since annihilation in the target material will dominate at low $Ps$ temperatures, while at high $Ps$ temperatures, the subsequent charge exchange cross-section (to form $\overline{H}$) drops rapidly [36]. The optimal velocity of $Ps$ is of the order of $10^4$ m/s. Since quantum confinement of $Ps$ within the pore limits the minimum achievable $Ps$ energy [37,38], by carefully tailoring the topology of the target material's pores, sufficient control of the $Ps$ velocity appears possible [37]. Ortho-$Ps$ fractions of the order of 40% have been obtained, also with targets formed of disordered $SiO_2$ structures (e.g. silica aerogel or compressed powder) [39]. We are currently evaluating the optimal converter material and $e^+$ energy in terms of ortho-$Ps$ yield, and are investigating how well the emitted $Ps$ is thermalized at very low target temperatures.

Photon energies close to the $Ps$ binding energy of 6.8 eV are required for photo-excitation to Rydberg states. Laser systems at the corresponding wavelengths (180 nm) are not commercially available. We therefore plan to perform a two-step excitation, from the ground state to the $n = 3$ state ($\lambda = 205$ nm), and then to the $n = 35$ Rydberg band ($\lambda \sim 1670$ nm) [40]. Two pulsed-laser systems, both of which are pumped by a Q-switched Nd:YAG laser (1064 nm, 4 ns, 140 mJ), are currently under development. Both systems must provide sufficient power to excite the emitted $Ps$ within a few ns and

must be geometrically matched to the expanding cloud. Furthermore, the bandwidths of the lasers must be tailored to the transition line-width, broadened due to the Doppler effect as well as level-split due to the motional Stark effect and the linear and quadratic Zeeman effect.

Antihydrogen formation will rely on the $Ps^* + \bar{p} \rightarrow \overline{H}^* + e^-$ resonant charge exchange process, where the star denotes a highly excited Rydberg state. The cross-section for this reaction scales approximately with the fourth power of the principal quantum number. The velocity distribution of antihydrogen formed with antiprotons at rest is dominated by the antiproton temperature, ideally that of the surrounding (cryogenic) environment [41], and the process ensures a narrow and well-defined band of quantum numbers. Our proposed technique is similar to a charge exchange technique based on Rydberg cesium [42], implemented successfully by ATRAP [43], but offers greater control of the final state distribution of antihydrogen atoms and, more importantly, allows pulsed production of cold antihydrogen. For 100 mK antiprotons, the formed antihydrogen has a velocity of $\sim$50 m/s before, and of several 100 m/s after acceleration. To reach such a low initial temperature, the Penning trap is coupled to a 50 mK dilution refrigerator.

While neutral atoms are not sensitive (to first order) to constant electric fields, they do experience a force when their electric dipole moment is exposed to an electric-field gradient. Since the dipole moment scales approximately with the square of the principal quantum number, Rydberg atoms are especially sensitive. Such Stark acceleration (and deceleration) has been successfully demonstrated, among others, with hydrogen after excitation to the $n = 22$, 23, 24 states [44,45]. In these experiments, accelerations of $2 \times 10^8$ m s$^{-2}$ were achieved: a hydrogen beam traveling at 700 m/s was stopped within 5 µs over a distance of only 1.8 mm. We intend to use a similar field configuration, generated by axially split electrodes within the cylindrical geometry of a Penning trap, to accelerate the formed antihydrogen atoms to about 400 m/s in the direction of the deflectometer apparatus.

In matter wave interferometers of the Mach–Zehnder type, three identical gratings are placed at equal distances $L$ from each other. The first two gratings produce an interference pattern with the same period $d$ as that of the gratings at the location of the third. Under the influence of gravity, the interference pattern is vertically displaced (it "falls") by a distance $\delta x = gT^2$ where $g$ is the local gravitational acceleration and $T$ is the time of flight $L/v$ of a particle beam traveling at velocity $v$. Contrary to such true interferometers, which place a very stringent limit on the acceptable beam divergence (and thus the antihydrogen temperature at production), the so-called Moiré deflectometer, in which diffraction on the gratings is replaced by a (classical) shadow pattern of those particles that converge onto the third grating, works in the classical regime. Interestingly, the gross characteristics of the interferometer are retained [46], in particular, the vertical displacement of the interference pattern. We intend to replace the third grating by a position-sensitive silicon strip detector (Fig. 3). Antihydrogen atoms impacting on the detector plane annihilate, and the impact point can be reconstructed by means of the energy deposited locally by the annihilation products.

The value of $g$ is extracted from two primary observables (time of flight $T$ and vertical displacement of the fringe pattern $\delta x$). The periodic nature of the arrangement means that for a given value of $T$ the impact point will have dropped by a well-defined amount $\delta x$ modulo the grating period. By varying the accelerating field gradient (and thus varying the velocity of the antihydrogen atoms), or simply through the spread in velocity of the ensemble of antihydrogen atoms, the quadratic dependence of $\delta x$ on $T$ is probed.

Our simulations have shown that in order to perform a measurement of $g$ to 1% relative precision, about $10^5$ antihydrogen atoms at a temperature of 100 mK will be required, equivalent to several months of data taking at the AD. In these simulations, a grating period of 80 µm was used, and a finite detector resolution of 10 µm was taken into account. The experiment is charge symmetric, in the sense that if antiprotons are replaced with protons, it should be possible to produce an identical beam of hydrogen atoms, which can be used to evaluate systematic effects of the measurement. While their behavior is expected to be identical in almost all respects to that of antihydrogen, measuring the impact point of (ground state) hydrogen atoms with a precision of the order of a few micrometers represents a challenge that has not been solved to date; excited states however might be detectable to this accuracy. Which fraction of the produced Rydberg (anti)hydrogen atoms remains excited during their trajectory through the Moiré deflectometer is equally an open question.

## 4. Status report on investigations of the properties of naturally occurring gravitational eigenstates (Allan Ernest and Matthew P. Collins)

The experimental demonstration [14,15] that neutrons can form quantized states in the gravitational field of the Earth raises the question as to whether gravitational eigenstates might exist naturally elsewhere in the universe and indicates a need to examine in more detail their general theoretical properties. Despite the almost universal study of quantum theory applied to atomic and molecular states, only recently work has been done [47,48] to investigate the properties of hypothetical well-bound stationary states that should exist in deep gravitational central potential wells. Some of the predicted states in these wells might have properties that make them potential candidates for Dark Matter. It is possible to construct a formation scenario that allows for the existence of an 'all-baryonic' universe that is consistent with both BBN ratios and WMAP anisotropy observations [49]. In this, a halo composed of dark eigenstates can form in the potential well of supermassive primordial black holes [50,51] because interaction cross-sections for eigenstates differ dramatically from those for a thermalized gas undergoing acoustic oscillation, the accreting matter having self-similar $1/r^2$ profiles [52]. Particles with highly mixed eigenspectra remain in the low-density, weak-field regions as visible particles. A detailed study of the formation

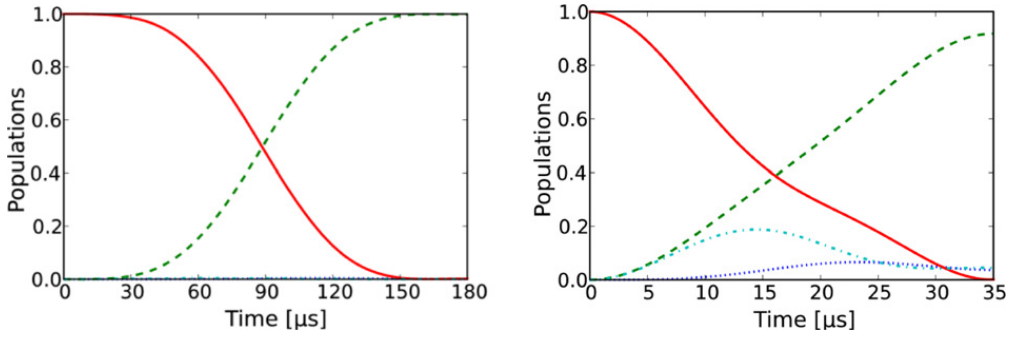


**Fig. 4.** Evolution of the occupation probability of the different momentum states as a function of time for a smooth standing-wave light pulse of duration 180 μs (left) and for a square-shaped pulse of duration 35 μs (right). Solid red line: $|-k_L\rangle$, dashed green line: $|+k_L\rangle$, dot-dashed light blue line: $|-3k_L\rangle$, dotted blue line: $|+3k_L\rangle$.

**Fig. 4.** Evolution de la probabilité d'occupation de différents états d'impulsion en fonction du temps pour une onde stationnaire lisse de durée 180 μs (à gauche) et pour un pulse de forme carrée de durée 35 μs (à droite). Ligne continue rouge : $|-k_L\rangle$, ligne discontinue verte : $|+k_L\rangle$, ligne pointillée-tiretée bleue : $|-3k_L\rangle$, ligne pointillée bleue : $|+3k_L\rangle$.

scenario and gravitational eigenstates' stability regarding to different types of de-excitation mechanisms is required and is in progress.

## 5. Classical and quantum trampoline for ultracold atoms (Thomas Bourdel, M. Robert-de-Saint-Vincent, J.-P. Brantut, Ch.J. Bordé, A. Aspect, P. Bouyer)

Cold atomic gases have proven to be a useful resource for precision measurements of the atom properties or of the external forces acting on them. For example, atom interferometers permit the measurement of the local gravity constant $g$ with a relative accuracy of the order of $10^{-8}$ at 1 s [53]. A long observation time is demanded in order to obtain the best accuracy. This time is limited not only by the expansion of the sample and thus its temperature (100 nK corresponds to an expansion velocity of $\sim$3 m/s for rubidium 87 and can be achieved by a combination of laser cooling and evaporative cooling techniques), but also by the size of the vacuum chamber in which the atoms are in free fall. In this paper, we describe two schemes producing atomic mirrors [54] in order to bounce the atoms upward in a controllable way and thus keep them in a small volume for a long time. These two schemes are hereafter called classical [55,56] and quantum trampolines [57].

The mirrors for both schemes are based on atom diffraction by a periodic optical potential [58], i.e. a vertical light standing wave of period $\frac{\pi}{k_L}$, where $k_L$ is the laser wave vector (in our case $\frac{2\pi}{k_L} = 780$ nm). An atom in the momentum state $|-k_L\rangle$ can be reflected to the state $|+k_L\rangle$ by a standing-wave laser pulse. This is a process called Bragg diffraction. After a time $T_0 = \frac{2\hbar k_L}{mg} \approx 1.2$ ms for $^{87}$Rb, where $\hbar$ is the reduced Planck constant and $m$ the atomic mass [59], the state $|+k_L\rangle$ evolves back into the state $|-k_L\rangle$ because of the downwards acceleration of gravity $g$. Repeating the standing-wave laser pulse with a period $T_0$ thus allows suspending the atoms at an almost constant altitude. It realizes a trampoline for ultracold atoms. This setup allows for the measurement of $g$ [55,56] as the trampoline only suspends atoms for the precise value of the period $T_0$.

We first analyze more precisely the diffraction process. The Hamiltonian $H$ of an atom in the presence of the standing wave and of gravity reads: $H = \frac{p^2}{2m} + mgz + V\sin^2(k_L z)$. In the absence of the standing wave ($V = 0$), a momentum state $|k\rangle$ evolves with time $t$ in $|k - \frac{gt}{\hbar}\rangle$. The interaction between the atoms and the optical potential leads to vertical momentum changes quantized in units of $2\hbar k_L$. Starting with a momentum state $|k\rangle$ at time $t = 0$, only the states $|k - \frac{gt}{\hbar} + 2nk_L\rangle$, where $n$ is an integer, will be populated over time. In this basis, the Hamiltonian reduces to a simple matrix with the energies $\frac{\hbar^2}{2m}(k - \frac{mgt}{\hbar} + 2nk_L)^2$ along the diagonal and $\frac{V}{4}$ as the coupling between the states differing by $2k_L$. The system dynamics can be simulated numerically.

To use the standing wave as a mirror, the idea is to use the resonant coupling between the states $|-k_L\rangle$ and $|+k_L\rangle$, which have the same energy. In this case a perfect mirror should be realizable. However, as the momentum states are constantly changing due to gravity, the resonant condition is only transiently met, reducing the possible duration of the pulse. In order to realize a good mirror (avoiding higher order diffraction), it is also favorable to use a smoothly varying intensity of the standing wave rather than square-shaped pulsed [60] (another possibility is to shape the pulse in a proper way to optimize diffraction to the reflected order [56]). In our case, we use a laser intensity varying as $\cos^2(\frac{\pi t}{\tau})$ between $t = -\frac{\tau}{2}$ and $\frac{\tau}{2}$, where $\tau$ is the total duration of the pulse and where the resonant condition is met at $t = 0$. For each value of $\tau$, the absolute value of the intensity is adjusted in order to obtain the maximum amount of transfer from the state $|-k_L\rangle$ to $|+k_L\rangle$. Theoretically, we find that $\tau = 170$ μs gives an optimum transfer efficiency (larger than 0.999). Fig. 4 shows the different state occupation probabilities as a function of time during the pulse.

In the experiment, we use $\tau = 180$ μs and are able to bounce a cloud of atoms 25 times corresponding to a total time of 30 ms (see [61] for details on the cold atom sample preparation). By varying the period $T$ between the laser pulses, we observe a resonance in the number of atoms kept on the trampoline [55,56] (see Fig. 5). This effect can be simply

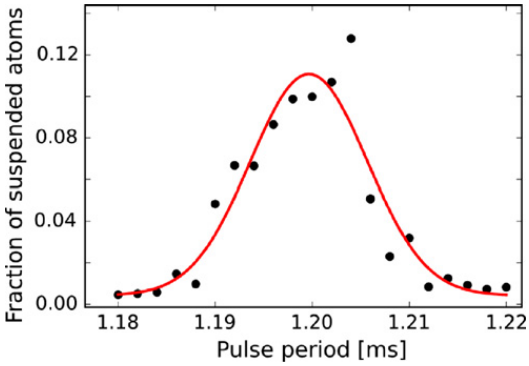


**Fig. 5.** Fraction of suspended atoms after 25 Bragg reflections using smooth light pulses as a function of the period $T$. Solid line: Gaussian fit to the data centered at $T = 1.1996$ µs, corresponding to $g = 9.81(1)$.

**Fig. 5.** Fraction d'atomes suspendus après 25 réflexions de Bragg avec des impulsions lumineuses lisses en fonction de la période $T$. Ligne continue : ajustement Gaussien des données centré en $T = 1{,}1996$ µs, correspondant à $g = 9{,}81(1)$.

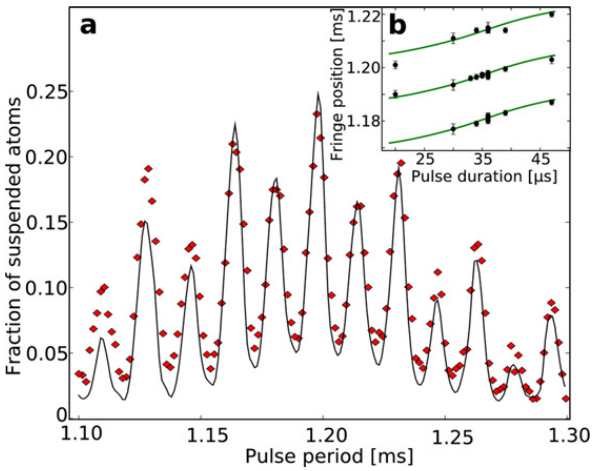


**Fig. 6.** (a) Fraction of suspended atoms after 10 square-shaped light pulses as a function of the period $T$. The overall envelope is due to the velocity selectivity [55] of the pulses as in the classical trampoline while the modulation is due to quantum interference. The solid line corresponds to a theoretical model [57]. (b) Position of three consecutive fringe maxima around the highest maximum, as a function of the pulse duration, showing the influence of the phase shift imprinted by the diffraction pulses. Dots are experimental points, with error bars reflecting the experimental uncertainties. Solid lines come from a theoretical model using $g = 9.815$.

**Fig. 6.** (a) Fraction d'atomes suspendus après 10 impulsions lumineuses carrées en fonction de la période $T$. L'enveloppe globale est due à la sélectivité en vitesse [55] des impulsions comme pour le trampoline classique, tandis que la modulation est due à l'interférence quantique. La ligne continue correspond à un modèle théorique [57]. (b) Position de trois maxima de frange consécutifs autour du plus haut maximum, en fonction de la durée de l'impulsion. Les points sont les valeurs expérimentales avec leurs barres d'erreur. Les lignes continues sont issues d'un modèle théorique supposant $g = 9{,}815$.

understood. If the period $T$ does not match $T_0$, the atoms have a mean residual acceleration and later laser pulses are applied on atoms with a momentum different from $-\hbar k_L$. The reflection probability is then reduced. From our experimental data, we can estimate $T_0$ and thus also give an estimate of the value of gravity $g = 9.81(1)$. This method does not rely on the phase between the different pulses as it is not an interferometer. We call it a classical trampoline (the word classical should be taken with a grain of salt as the diffraction process itself is quantum. The momentum transfer is quantized in units of $\hbar k_L$). The suspended atoms can then be used to build a two-path interferometer as demonstrated in [56].

Interestingly, our setup can also efficiently suspend atoms against gravity using shorter and square-shaped pulses [57]. This may seem surprising as in this case, the quality of an individual atomic mirror is poor. For example, for a 35 µs pulse acting on $|-k_L\rangle$, 93% of the atoms are transferred to $|+k_L\rangle$, but also 3% to $|-3k_L\rangle$ and to $|+3k_L\rangle$ and a fraction below 1% remains in $|-k_L\rangle$. Experimentally, in this case, we observe that (unlike in the smoothed pulse case) the fraction of suspended atoms shows fringes as a function of $T$ (see Fig. 6). This behavior is characteristic of an interferometer. These interferences actually arise from the recombination of the various trajectories populated due to the splitting induced by the imperfect mirror pulses, as detailed in [57] and similarly to the theoretical proposition [62]. This method thus permits to simultaneously suspend the atoms against gravity and create an interferometer. Actually, one can use the absolute fringe position for a measurement of gravity, as in standard atom gravimeters. In order to do that, one has to be able to predict the phase acquired during the laser pulses (using the diffraction model presented previously). For example, the phase of the interferometer varies with the laser pulse duration $\tau$. Here we find $g = 9.815(4)$ in agreement with the expected value in Palaiseau (the slight change from the previously published value [57] is due to use of the precise value [59] of $\frac{\hbar}{m}$ for $^{87}$Rb rather than $m = 87m_a$, where $m_a$ is the atomic mass).

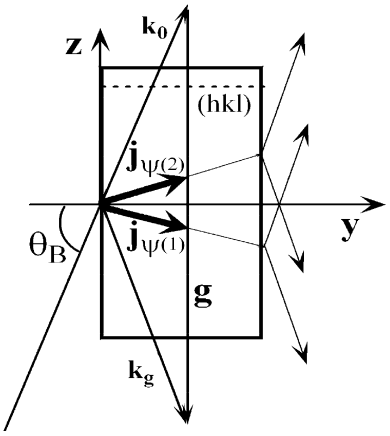


**Fig. 7.** Symmetrical Laue diffraction scheme for finite perfect crystal. $\mathbf{j}_{\psi^{(1)}}$ and $\mathbf{j}_{\psi^{(2)}}$ are the neutron fluxes ("Kato trajectories") for two Bloch waves.

**Fig. 7.** La diffraction de Laue symétrique pour un cristal fini parfait. $\mathbf{j}_{\psi^{(1)}}$ et $\mathbf{j}_{\psi^{(2)}}$ sont les flux de neutrons (« trajectoires de Kato ») pour deux ondes de Bloch.

In conclusion, we have shown methods to suspend atoms against gravity using a standing wave as an atomic mirror. Using smoothed standing-wave laser pulses, very efficient reflection is expected and the atoms are suspended as on a trampoline. Alternatively, short square-shaped laser pulses lead to numerous possible atom trajectories, which then interfere. The atoms may then efficiently bounce due to quantum interferences hindering the losses. In this case, our setup is a quantum trampoline [57], a multiple-wave interferometer [63–65] permitting the measurement of gravity. Our work opens perspectives for new types of compact interferometers, in which atoms do not fall over an extended distance.

We acknowledge F. Moron and A. Villing for technical assistance, R.A. Nyman, J.-F. Clément, and B. Allard for their work on the apparatus, F. Impens for helpful discussions. This research was supported by CNRS, CNES as part of the ICE project, Direction Générale de l'Armement, the project "blanc" MélaBoFérIA from ANR, IFRAF, by the STREP program FINAQS of the European Union and by the MAP program SAI of the European Space Agency (ESA).

## 6. Eötvös-type experiment with cold neutrons (Vladimir V. Voronin, V.V. Fedorov, I.A. Kuznetsov, E.G. Lapin, S.Yu. Semenikhin, Yu.P. Braginetz, E.O. Vezhlev)

The aim of this experiment is to measure the ratio of the inertial to gravitational neutron masses with an accuracy about $\sigma(m_i/m_G) \sim 10^{-6}$ using Laue diffraction in a perfect crystal.

There is a well known effect of diffraction enhancement when a small variation of the incident beam direction leads to a considerable deflection of a neutron trajectory inside a crystal [66]. The neutron in the crystal changes the momentum direction by the angle of $2\theta_B$ (by several tens degrees) while the incident neutron beam deflects by the Bragg width (within a few arc seconds) [66]. Such effect was used to probe the magnetic charge of neutron [67]. There are some proposals to utilize this effect for measuring a neutron charge [68] and for the investigation of gravitational properties of a neutron falling in the Earth field [69].

The influence of gravity on neutron diffraction in a deformed single crystal was firstly observed in the work [70]. The effect of gravity on a neutron was investigated before by using the neutron interferometer [3,71] and diffraction grating [72]. Recently an essential increase of the neutron stay time in a crystal for the Bragg angles close to $\pi/2$ has been observed at the WWR-M reactor (PNPI, Gatchina) [73]. Any effect related to an external affect on a neutron should depend on the interaction time, so we expect a considerable increase of sensitivity to a small external affect for Bragg angles close to the right one.

Here we will consider the symmetrical Laue diffraction scheme in a transparent crystal with the system of crystallographic planes described by the reciprocal lattice vector $\mathbf{g}$ normal to the planes (see Fig. 7), $g = 2\pi/d$, $d$ is the interplanar distance. In this case, the neutron wave function in a crystal will be a superposition of two Bloch waves $\psi^{(1)}$ and $\psi^{(2)}$ corresponding to two branches of the dispersion surface [74].

Any deformation of a crystal means that the value and/or direction of vector $\mathbf{g}$ are different for the crystal different points, i.e. $\mathbf{g}$ depends on the spatial coordinates $Y$ and $Z$. Neutron Laue diffraction in a weakly deformed crystal can be described by the so-called "Kato forces" [75], which are directed along the reciprocal lattice vector $\mathbf{g}$ and their values are determined by the value of crystal deformation [70]:

$$f_k(y,z) = -\frac{k_0}{4\cos\theta_B}\left(\frac{\partial}{\partial z} + \frac{1}{c}\frac{\partial}{\partial y}\right)\alpha(y,z) \tag{17}$$

where $k_0$ is the neutron wave vector in the crystal, $\theta_B$ is the Bragg angle,

$$\alpha(y,z) = \frac{g^2 + 2(\mathbf{k}_0 \cdot \mathbf{g})}{k_0^2} \tag{18}$$

is the parameter of deviation from the exact Bragg condition. Eq. (17) is valid for crystal deformations small as compared with the diffraction Bragg width.

The neutron "Kato trajectories" for two kinds of Bloch waves in the crystal (describing a behavior of the neutron density fluxes $\mathbf{j}_{\psi^{(1)}}$ and $\mathbf{j}_{\psi^{(2)}}$) are determined by the equation

$$\frac{\partial^2 z}{\partial y^2} = \pm \frac{c}{m_0} f_k(y, z) \tag{19}$$

here $c \equiv \tan\theta_B$ and $m_0 \equiv 2F_g d/V$ is the so-called "mass Kato", $F_g$ is the neutron structure amplitude, $V$ is the unit cell volume. The sign $\pm$ in Eq. (19) corresponds to different Bloch waves.

As it follows from Eqs. (17) and (18) the "Kato force" arises due to the dependence of the deviation parameter $\alpha$ on the spatial coordinates $Z$ and $Y$. Therefore if we put the undeformed perfect crystal in a certain field of the force affecting the neutron along reciprocal lattice vector $\mathbf{g}$, we will have the same result as for the deformed crystal. The external field affect on a diffracting neutron was considered in [71] and influence of gravity on neutron diffraction in an elastically bent crystal was experimentally observed [69].

It is easy to show that the external force $F_{ext}$ affecting the neutron along the vector $\mathbf{g}$ ($Z$ axis, see Fig. 7) is equivalent to the gradient of interplanar distance with the value

$$\xi_f = \frac{F_{ext}}{2E_n} \tag{20}$$

where $E_n$ is the neutron energy.

Therefore the neutron trajectory equation in the crystal in the presence of external field will have the form

$$\frac{\partial^2 z}{\partial y^2} = \pm \frac{c^2 g}{2m_0} \frac{F_{ext}}{2E_n} \tag{21}$$

Let us compare this equation for the "Kato trajectory" with that for a usual trajectory of a neutron under the same external field in free space. The last one is described by usual Newtonian equation which has the form

$$\frac{\partial^2 z}{\partial y^2} = \frac{F_{ext}}{2E_n} \tag{22}$$

As it follows from Eqs. (21) and (22) the "curvature" of the diffracting neutron trajectory in the crystal is magnified by the factor

$$K_e = \pm \frac{c^2 g}{2m_0} \tag{23}$$

This factor depends on the Bragg angle as $c^2 \equiv \tan^2\theta_B$, so for the Bragg angles $\theta_B \approx (84\text{–}88)^\circ$ influence of deformation can be intensified by a factor $\sim$100–1000 as compared with the Bragg angle $\sim 45^\circ$.

The numerical calculation of factor $K_e$ for (110) and (200) quartz planes gives

$$K_e^{(110)} = \pm 0.7 \times 10^8 \tag{24}$$

$$K_e^{(200)} = \pm 0.6 \times 10^9 \tag{25}$$

for the Bragg angle $\theta_B = 87^\circ$ ($c = 20$).

Therefore, the 10 cm crystal is for the trajectory curvature equivalent to $\sim$1 km of free flight. The diffraction enhancement of the angular deflection of a neutron trajectory inside a crystal is well known, see for instance [66], but we have to note that such an effect can be considerably magnified by an additional gain factor proportional to $\tan^2\theta_B$ for the Bragg angles close to $\pi/2$ [76]. The observed effects give us a chance to build up a device with unprecedented sensitivity to an external force affected the neutron.

One of the applications can be connected with the measurement of the ratio of inertial to gravitational neutron masses. Our Earth is moving at the stationary orbit around the Sun, it means that the gravitational force proportional to the gravitational mass is in balance with the centrifugal force proportional to the inertial mass. If it is not the case for neutrons, then in the coordinate system connected with the Earth the neutron will see the non-zero force[1]

$$F_m = \frac{(m_i - m_G) \cdot GM_S}{R_S^2} \tag{26}$$

where $m_G$ and $m_i$ are the neutron gravitational and inertial masses, $G$ is the gravitational constant, $M_S$ is the Sun mass and $R_S$ is the distance to the Sun. Moreover, this force will oscillate in the laboratory coordinate system with a one day period

[1] The idea of this experiment is an analogue to the well known Eötvös experiment for the equivalence principle checking [77].

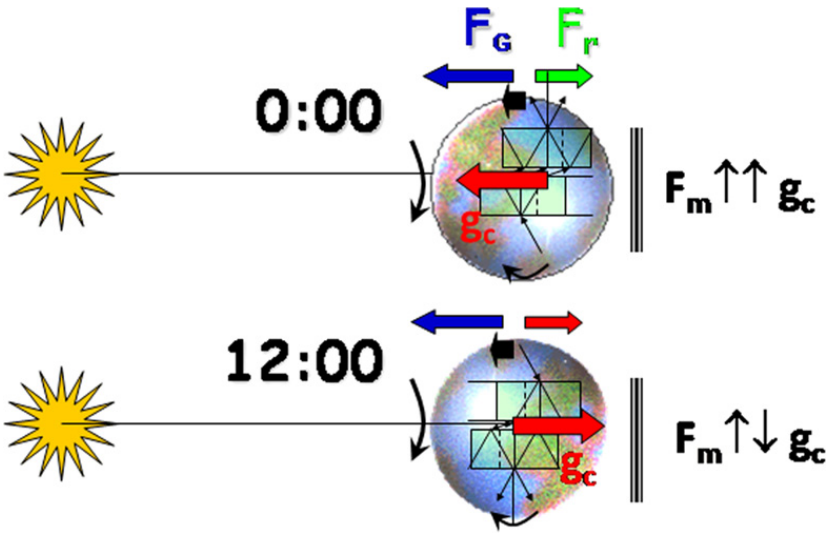


**Fig. 8.** Idea of the experiment.

**Fig. 8.** Principe de l'expérience.

due to the Earth spinning motion, see Fig. 8. Preliminary estimations demonstrate that available silicon and quartz crystals and flux of modern neutron sources allow reaching the sensitivity

$$\sigma(m_i/m_G) \sim \left(10^{-5}\text{–}10^{-6}\right) \tag{27}$$

that is about two orders better than the current accuracy [78]. Of course to reach such sensitivity we should control the angular crystal position relatively the local gravity force with accuracy about $(10^{-8}\text{–}10^{-9})$, that can be done by the angular inclinometer. Technical details of the experiment are discussed in [79].

This work is supported by RFBR (grant No. 08-02-00313).

## 7. Problems to measure confinement-induced neutron phases (Hartmut Lemmel, H. Rauch)

Neutrons transmitted through narrow slits become slowed down due to a transverse quantization of their wave function, which causes a measurable phase shift in neutron interferometry experiments [80,81]. For the slit width in the order of 20 µm the related energy levels are in the peV-range and the expected phase shift in a 2 cm long channel is in the order of 2 degrees. First measurements showed the effect [82] but further experiments at ILL and NIST showed mostly phase shifts larger than expected which remain unexplained. The wave function within and behind the slits has been calculated in detail and the wave function structure of a perfect crystal interferometer has been taken into account. Still a discrepancy between measured and calculated values remains. Several ideas are discussed, such as phase shift contributions by the channel walls, phase shift contributions by slit diffracted wave components, and short-range non-Newtonian gravitational forces.

## 8. Conclusion

The common feature of various experiments/methods considered here is that they involve quantum phenomena in a gravitational field. Considering them together, however, we could learn that they have many common points both in physics and in methodology.

## References

[1] S. Schlamminger, et al., Phys. Rev. Lett. 100 (2008) 041101.
[2] J. Overduin, et al., Adv. Space Res. 43 (2009) 152.
[3] R. Colella, et al., Phys. Rev. Lett. 34 (1975) 1472.
[4] H. Rauch, et al., Nature 417 (2002) 630.
[5] M. Kasevich, et al., Appl. Phys. B 54 (1992) 321.
[6] K.Y. Chung, et al., Nature 400 (1999) 849.
[7] S. Fray, et al., Phys. Rev. Lett. 93 (2004) 240404.
[8] G. Gabrielse, et al., Phys. Rev. Lett. 100 (2008) 113001.
[9] G.B. Andersen, et al., Nature 468 (2010) 673.
[10] J. Sherk, Phys. Lett. B 88 (1979) 265.
[11] C.L. Cesar, et al., AIP Conf. Proc. 770 (2005) 33.
[12] G. Gabrielse, et al., CERN-SPSC-2010-006/SPSC-SR-057.
[13] A. Kellerbauer, et al., Nucl. Instrum. Methods Phys. Res., Sect. B 266 (2008) 351.

[14] V.V. Nesvizhevsky, et al., Nature 415 (2002) 297.
[15] V.V. Nesvizhevsky, et al., Phys. Rev. D 67 (2003) 102002.
[16] V.V. Nesvizhevsky, et al., Europ. Phys. J. C 40 (2005) 479.
[17] J.E. Lennard-Jones, Trans. Faraday Soc. 28 (1932) 333.
[18] H.B. Casimir, et al., Phys. Rev. 73 (1948) 360.
[19] I.E. Dzyaloshinskii, et al., Adv. Phys. 10 (1960) 165.
[20] A.Yu. Voronin, et al., J. Phys. B 38 (2005) 301.
[21] A.Yu. Voronin, et al., Phys. Rev. A 72 (2005) 062903.
[22] A.Yu. Voronin, et al., Phys. Rev. A 83 (2011) 032903.
[23] A.Yu. Voronin, et al., Phys. Rev. D 73 (2006) 044029.
[24] M. Abramowitz, I.A. Stegun, Handbook of Mathematical Functions, 10th edition, Dover Publications, New York, 1972.
[25] L.I. Schiff, Phys. Rev. Lett. 1 (1958) 254.
[26] L.I. Schiff, Proc. Natl. Acad. Sci. 45 (1959) 69, http://www.pnas.org/cgi/reprint/45/1/69.
[27] R.J. Hughes, et al., Phys. Rev. Lett. 66 (1991) 854.
[28] M. Amoretti, et al., ATHENA Collaboration, Nature 419 (2002) 456.
[29] G. Gabrielse, et al., ATRAP Collaboration, Phys. Rev. Lett. 89 (2002) 213401.
[30] http://aegis.web.cern.ch/aegis.
[31] L.V. Jorgensen, et al., ATHENA Collaboration, Phys. Rev. Lett. 95 (2005) 025002.
[32] G. Gabrielse, et al., ATRAP Collaboration, Phys. Lett. B 548 (2002) 140.
[33] G. Andersen, et al., ALPHA Collaboration, Phys. Rev. Lett. 105 (2010) 013003.
[34] U. Warring, et al., Phys. Rev. Lett. 102 (2009) 043001.
[35] D.W. Gidley, et al., Annu. Rev. Mater. Res. 36 (2006) 49.
[36] C. Canali, publication in preparation.
[37] S. Mariazzi, et al., Phys. Rev. B 78 (2008) 085428.
[38] P. Crivelli, et al., Phys. Rev. A 81 (2010) 052703.
[39] R. Ferragut, et al., J. Phys.: Conf. Ser. 225 (2010) 012007.
[40] F. Castelli, et al., Phys. Rev. A 78 (2008) 052512.
[41] B.I. Deutch, et al., Hyperfine Interact. 76 (1993) 153.
[42] E.A. Hessels, et al., Phys. Rev. A 57 (1998) 1668.
[43] C.H. Storry, et al., ATRAP Collaboration, Phys. Rev. Lett. 93 (2004) 263401.
[44] E. Vliegen, et al., Phys. B 39 (2006) L241.
[45] E. Vliegen, et al., Phys. Rev. A 76 (2007) 023405.
[46] M.K. Oberthaler, et al., Phys. Rev. A 54 (1996) 3165.
[47] A.D. Ernest, J. Phys. A: Math. Theor. 42 (2009) 115207.
[48] A.D. Ernest, J. Phys. A: Math. Theor. 42 (2009) 115208.
[49] A.D. Ernest, A quantum approach to dark matter, in: Val Blain (Ed.), Dark Matter: New Research, NOVA Science Publishers, New York, 2006.
[50] B.J. Carr, Astrophys. J. 201 (1975) 1.
[51] N. Afshordi, et al., Astrophys. J. 594 (2003) L71.
[52] E. Bertschinger, Astrophys. J. Suppl. 58 (1985) 39.
[53] A. Peters, et al., Metrologia 38 (2001) 25.
[54] C.G. Aminoff, et al., Phys. Rev. Lett. 71 (1993) 3083.
[55] F. Impens, et al., Appl. Phys. B 84 (2006) 603.
[56] K.J. Hughes, et al., Phys. Rev. Lett. 102 (2009) 150403.
[57] M. Robert-de-Saint-Vincent, et al., Europ. Phys. Lett. 89 (2010) 10002.
[58] M. Kozuma, et al., Phys. Rev. Lett. 82 (1999) 871.
[59] P. Clade, et al., Phys. Rev. A 74 (2006) 052109.
[60] C. Keller, et al., Appl. Phys. B 69 (1999) 303.
[61] J.-F. Clement, et al., Phys. Rev. A 79 (2009) 061406.
[62] F. Impens, et al., Phys. Rev. A 80 (2009) 031602.
[63] M. Weitz, et al., Phys. Rev. Lett. 77 (1996) 2356.
[64] H. Hinderthür, et al., Phys. Rev. A 59 (1999) 2216.
[65] T. Aoki, et al., Phys. Rev. A 63 (2001) 063611.
[66] A. Zeilinger, et al., Phys. Rev. Lett. 57 (1986) 3089.
[67] K. Finkestein, et al., Physica B 136 (1986) 131.
[68] Yu. Alexandrov, in: Proc. ISINN-XIII, 2006, p. 166.
[69] S.A. Werner, Phys. Rev. B 21 (1980) 1774.
[70] V.L. Alexeev, et al., JETP 94 (1988) 371.
[71] J.-L. Staudenmann, et al., Phys. Rev. A 21 (1980) 1419.
[72] A.I. Frank, et al., JETP Lett. 86 (2007) 255.
[73] V.V. Voronin, et al., JETP Lett. 71 (2000) 76.
[74] H. Rauch, D. Petrachek, in: H. Duchs (Ed.), Neutron Diffraction, Springer, Berlin, 1978, pp. 303–351.
[75] N. Kato, J. Phys. Soc. Japan 19 (1964) 971.
[76] V.V. Fedorov, et al., JETP Lett. 85 (2007) 82.
[77] R.V. Eötvös, et al., Annal. Physik 68 (1922) 11.
[78] J. Schmiedmayer, Nucl. Instrum. Methods Phys. Res., Sect. A 284 (1989) 59.
[79] V.V. Voronin, et al., PNPI preprint 2849 (Gatchina, 2010, 28).
[80] J.M. Levy-Leblond, Phys. Lett. A 125 (1987) 441.
[81] D.M. Greenberger, Physica B 151 (1988) 374.
[82] H. Rauch, et al., Nature 417 (2002) 630.